J MATER RES TECHNOL. 2019;8(3):2565–2572

Available online at www.sciencedirect.com

jmr&t
Journal of Materials Research and Technology
www.jmrt.com.br

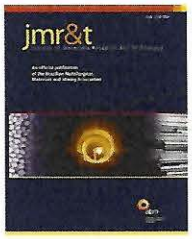

Original Article

Mullite cytotoxicity and cell adhesion studies

Leandro Fernandes[a], *Renata Aquino de Carvalho*[b], *Andre Capaldo Amaral*[b], *Edison Pecoraro*[c], *Rafael Salomão*[a], *Eliane Trovatti*[b,*]

[a] *Materials Engineering Department – São Carlos School of Engineering, University of São Paulo, Avenida Trabalhador São-carlense 400, CEP: 13566-590, São Carlos, SP, Brazil*

[b] *University of Araraquara – UNIARA, Rua Carlos Gomes, 1217, CEP: 14801-340, Araraquara, SP, Brazil*

[c] *São Paulo State University (UNESP), Institute of Chemistry, CEP: 14800-060, Araraquara, SP, Brazil*

ARTICLE INFO

Article history:
Received 28 July 2018
Accepted 1 April 2019
Available online 15 May 2019

Keywords:
Mullite
Human cell
Cytotoxicity studies
Adhesion tests
Mechanical properties

ABSTRACT

Mullite is a low cost ceramic material based on aluminous silicate and synthesized *via* solid state reaction. Mullite displays potential properties for application in the biomedical field, specially its high mechanical strength, however it is poorly characterized with respect to its specific cytotoxicity and capability to allow the cell adhesion to its surface. Here, mullite was prepared by sintering the mixture of Al_2O_3 and SiO_2 at 1500 °C and characterized. Its elastic modulus was 135 GPa and its flexural strength, 109 MPa. The study of the viability of GM07492 human cells in presence of mullite revealed the proliferation and adhesion of the cells on its surface, which is an indication of biocompatibility. Its good mechanical properties and cytocompatibility suggested that mullite can be used as an alternative material for biomedical applications and dentistry.

1. Introduction

Ceramic materials have been extensively used in medicine due to their biocompatibility, high stiffness and compression strength ideal for use in orthopedic implants. Classical examples of ceramics used for bone replacement are alumina (Al_2O_3) [1,2] and zirconium dioxide (ZrO_2) based biomaterials [3–6]. Al_2O_3 is an important commercially available biomaterial, however its low fracture toughness represents a great drawback. ZrO_2 undergoes aging at body temperature in liquid medium, which limit its use in internal prostheses [7–9]. Although their association generate several devices for medical use (mainly for bone replacement), clinical data in orthopedics have demonstrated the need to develop new biomaterials with improved properties for good long-term performance [10–13].

Mullite ($3Al_2O_3{\cdot}2SiO_2$) is a low cost aluminous silicate with 71.8 wt% Al_2O_3 and 28.2 wt% SiO_2 [14], representing one of the main raw materials for the ceramic industry. Its application for development of new products for biomedical use is a strategy to decrease the costs, which also overcome the limitation [15]. Mullite is the result of the treatment of silica (SiO_2) and alumina (Al_2O_3) [16] at temperatures above 1200 °C forming its typical crystalline phase. Many sources of SiO_2 can be used for mullite synthesis, including the SiO_2 extracted from the silicon elemental purification process, a high available raw material, also known as microsilica. Usually mullite is found in

* *Corresponding author.*
E-mail: elianetrov@yahoo.com.br (E. Trovatti).

https://doi.org/10.1016/j.jmrt.2019.04.001

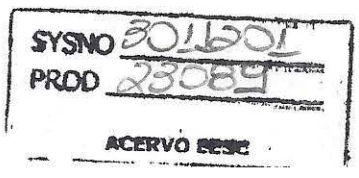

applications that require high mechanical strength and high melting point, such as refractory materials [17,18], catalysts and filters in general [19,20]. Mullite avoids crack because it does not display phase transitions and volume expansion. This feature overcomes the drawbacks of conventional ceramics, which shows phase transition and can crack when expand [21].

Mullite derivatives have arisen for applications in medicine [22]. For instance, the apatite–mullite glass-ceramic [23] produced *via* selective laser sintering allowed bone growth into its porous structure after implanting in rabbit tibiae for four weeks [24]. The material did not show *in vitro* cytotoxic effect for the human dermal fibroblasts [25]. In another study, the biphasic composite based on mullite and calcium phosphate led to good cell viability, proliferation, and osteoblastic differentiation, which suggests it could be used for orthopedic applications [22]. Hydroxyapatite–mullite ceramic material, another mullite derivative induced cytotoxic and genotoxic activity against L929 mouse fibroblast cells. The authors attributed the negative effect to the particle size, concentration and composition of mullite [26]. All the mullite derivatives are glass ceramic based on calcium and/or phosphate salts found in the biological environment that perform biological holes, resulting in bioactive surface materials, which can improve their biological compatibility. However, their mechanical properties are decreased by these salts in their formulations. The compromise between mechanical properties and biocompatibility is crucial for materials designed for biomedical applications. Mullite shows good mechanical properties, avoids cracks and is expected to be inert. This is a good combination of properties for its use in the development of materials for biological purposes. Although, to the best of our knowledge, its biological properties, such as cytotoxicity and cell adhesion is not described in the literature, encouraging the development of this work.

In this study, mullite was synthetized from synthetic amorphous silica associated with calcined alumina and characterized for biomedical applications. The *in vitro* biocompatibility was accessed testing the viability of human cells in the presence of mullite by MTT cytotoxicity assay, and the adhesion of human cells on the surface of the material. The *in vitro* cytotoxicity assays were studied here as the first level of evidence tests for biomedical applications of mullite.

2. Materials and methods

2.1. Materials

The materials used for the preparation of the mullite were (a) alumina (A1000SG, Almatis, Germany), (b) amorphous silica obtained by steam precipitation of elemental silicon (Microsilica 971, Elkem, Norway), organic binder (PVB; Polyvinyl butyral, Butivar® 98, Sigma-Aldrich, USA) and isopropyl alcohol (Synth; Brazil). The materials used for the biological tests were Dulbecco's modified eagle's medium (DMEM) and fetal bovine serum (Nutricell) purchased from (Gibco/Thermofisher), penicillin and

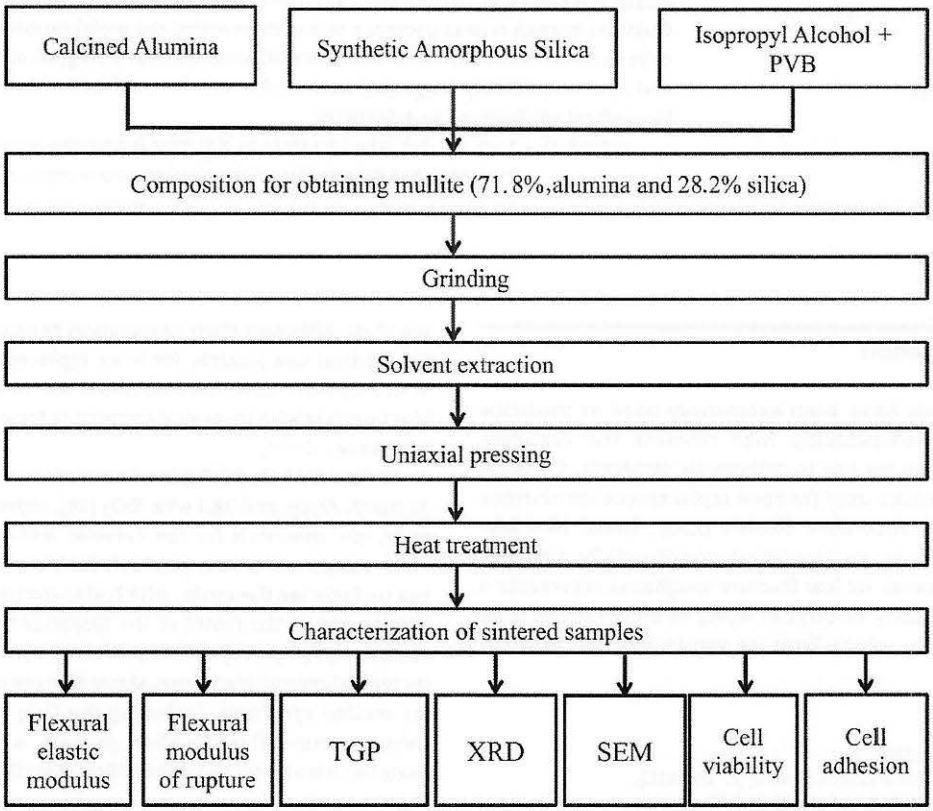

Fig. 1 – Scheme of the experimental procedure of mullite preparation and characterization.

Table 1 – Characteristics of raw materials.

Physico-chemical properties	Microsilica[a]	Alumina[b]	Method and equipment
Specific surface area (SSA; $m^2 g^{-1}$)	24	9.4 ± 0.56[c]	BET method, in a Quantachrome Autosorb 1200e, Quantachrome Instruments, USA
Total pore volume (TPV; $cm^3 g^{-1}$)	0.050	2.17 ± 0.33[c]	
Particle size (D_{50}/D_{90}, μm)	0.086/0.12	0.75/2.9	Particle size distribution (DT-1202, Dispersion Technology Inc., USA)
Composition (wt%)	SiO_2: 94.988 Al_2O_3: 4.242 CaO: 0.242 SO_3: 0.236 K_2O: 0.196 Fe_2O_3: 0.064 ZnO: 0.015 MnO: 0.013 PdO: 0.003	Al_2O_3: 99.818 Na_2O: 0.090 Fe_2O_3: 0.029 CaO: 0.044 ZnO: 0.007	X-ray dispersive spectroscopy, Shimadzu, EDX 720, Japan

[a] Microsilica U971, Elkem, Norway.
[b] Alumina, A1000SG; Almatis, USA.
[c] Average value of five measurements and standard deviation.

streptomycin 10 U/mL (Sigma Aldrich), 3-(4,5-dimethylthiazol-2-yl)-2,5-diphenyltetrazolium salt (MTT) from Merck, isopropyl alcohol, dimethyl sulfoxide, sodium hydroxide, sodium hypochlorite (NaClO) and phosphate buffer saline (PBS) purchased from Synth; trypsin from Gibco, 4,6-Diamidino-2-phenylindole (DAPI) and fluorescein isothiocyanate (FITC) from Sigma Aldrich. All solvents and reagents (analytical grade) were used as purchased. GM07492 cell line (human fibroblast primary cell line) was purchased from GM07492 Coriell Cell Repository (NIGMS Human Genetic Cell Repository), New Jersey, USA.

2.2. Methods

2.2.1. Preparation and characterization of mullite

Dried silica and alumina were mixed in a stoichiometric proportion and dispersed in 2 wt% PVB solution in isopropyl alcohol to form a suspension containing 33 wt% of solids for the mullite formulation ($3Al_2O_3{\cdot}2SiO_2$). The suspension was poured into a high density polyethylene flask (2 L) for grinding with zirconia spheres (5 mm diameter, mass ratio of sphere: powder 10:1) at 90 rpm for 2 h. Isopropyl alcohol evaporated and the powder with PVB binder was de-agglomerated ($D_{part} < 100$ μm) and pressed under uniaxial compression at 40 MPa for generating bars (6 × 20 × 70 mm) and cylinders (13 mm diameter × 3 mm width). A heating treatment was applied at 5 °C min^{-1} heating rate, hold at 1500 °C for 3 h; cooling rate of 10 °C min^{-1}. The scheme of the mullite preparation is shown in Fig. 1.

The flexural elastic modulus of the mullite samples was determined by the impulse excitation technique (Sonelastic equipment, PTCA, Brazil) according to ASTM C 1198-91. The flexural modulus of rupture at three points was carried out in a universal testing machine (Model WDW-30E, China) equipped with a 5 kN load cell and at of 0.5 mm min^{-1} crosshead speed according to ISO 6872 [27]. Prior to each measurement, the specimen dimensions were measured by a high precision digital caliper of 0.01 mm accuracy.

The average values of flexural modulus of rupture were calculated by Eq. (1) after 5 measurements:

$$\sigma = \frac{3Pl}{2wb^2} \quad (1)$$

where P is the rupture load in N, l is the test span (center-to-center distance between support rollers) in mm, w is the width of the specimen in mm, and b is the thickness of the specimen in mm.

The samples used in the mechanical tests were pulverized in an agate mortar ($D_{90} < 100$ μm), dried at 120 °C for 12 h and used to determine the density (ρ; g cm^{-3}) using helium pycnometer (Ultrapycnometer 1200e, Quantachrome Instruments, USA). Each density value was the average of five consecutive measurements. The total geometric porosity (TGP; %) was determined by Eq. (2):

$$\text{TGP} \quad (\%) = 100 \times \left[1 - \frac{M_{solid}/LWT}{\rho}\right] \quad (2)$$

where TGP = total geometric porosity (%), M_{solid} = mass of the solid, L = bar length (cm), W = bar width (cm), T = bar thickness (m) and ρ = solid density (g cm^{-3}).

X-ray diffraction was applied in the 2θ range from 3° to 100° and read at 2° per minute speed by a Rigaku Rotaflex diffractometer, model RV 200B, Japan. The Rietveld refinement [28] method quantified the crystalline phases and the powder that determined the density was also used for X-ray diffraction.

Scanning electron microscopy (SEM) (FEI Inspect F50, Netherlands microscope) was used to determine the morphology of the fracture sections of the samples after the flexural test, as well the morphology of the raw materials. The samples were coated with evaporated carbon using a Q150R Quorum Technologies, UK sputter.

2.2.2. Biological tests

Cell culture – Human cells GM07492 (1×10^3 cells/mL) were incubated in a DMEM culture medium supplemented with fetal bovine serum (10 vol%) and antibiotics (penicillin 10 U/mL; streptomycin 0.1 mg/mL). They were incubated at 37 ± 2 °C in 5% CO_2 atmosphere until reaching 80–90% confluence for seeding the ceramic samples. The GM07492 line is a useful cell line model for studies of adverse cellular effects, as *in vitro* cytotoxicity, and also as pre-osteoblastic cell in contact with implants in the body.

Cell viability – Cell viability and cell adhesion studies were carried out as the preliminary tests of the mullite biocompatibility. MTT is an indicative test for measuring the mitochondrion dehydrogenase activity (MTT is reduced by NADH to a purple formazan salt). The formazan represents a quantifiable marker for living cells, measured by absorption. For the test the ceramic cylinders were immersed in 24-well plates and the cells (1.5×10^4 cells/mL, 1 mL) were seeded on the surface of each cylinder, which were kept at 37 ± 2 °C in a

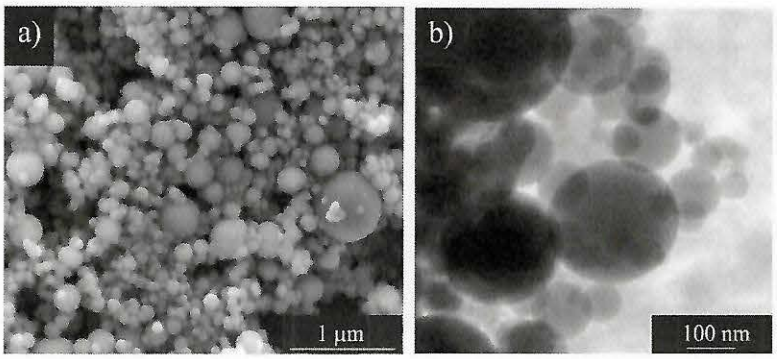

Fig. 2 – (a) SEM and (b) TEM for commercial silica Microsilica.

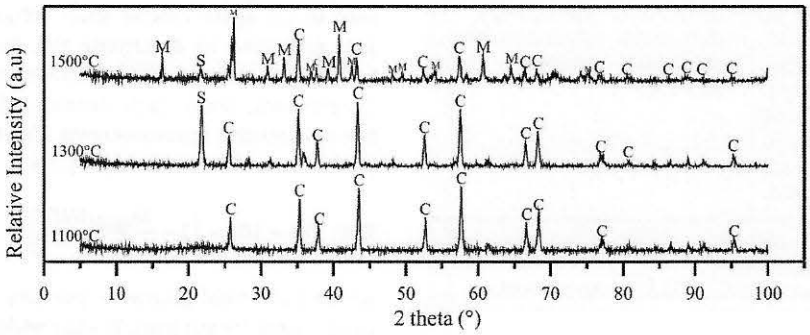

Fig. 3 – X-ray diffraction pattern of mullite obtained at 1500 °C. JCPDS file used for identification: C – corundum (JCPDS 42-1468); S – cristobalite (JCPDS 39-1425); M – mullite (JCPDS 15-0776).

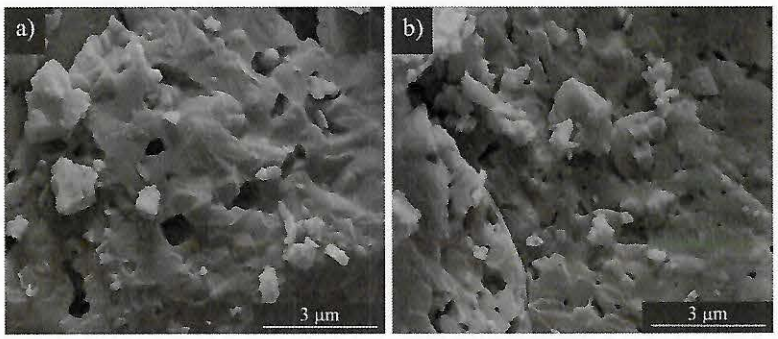

Fig. 4 – Fracture surface of mullite treated at 1500 °C.

Table 2 – Mechanical properties of mullite.

Materials	Mechanical properties			Reference
	Elastic modulus (GPa)	Flexural strength (MPa)	Total porosity (%)	
Mullite	135 ± 4.1	109 ± 5	7.8 ± 0.71	Present study
Materials for similar applications		Hydroxyapatite		[30]
	7 GPa	48 MPa	Not Determined	
		Zirconia toughened alumina (ZTA)		
	289 GPa	414 MPa	Not Determined	
		Zirconia		
	200 GPa	711	Not Determined	
		CaP–mullite (20–30 wt%)		[31]
	60–80 GPa	75–80	Not Determined	
	72 GPa	93	Not Determined	

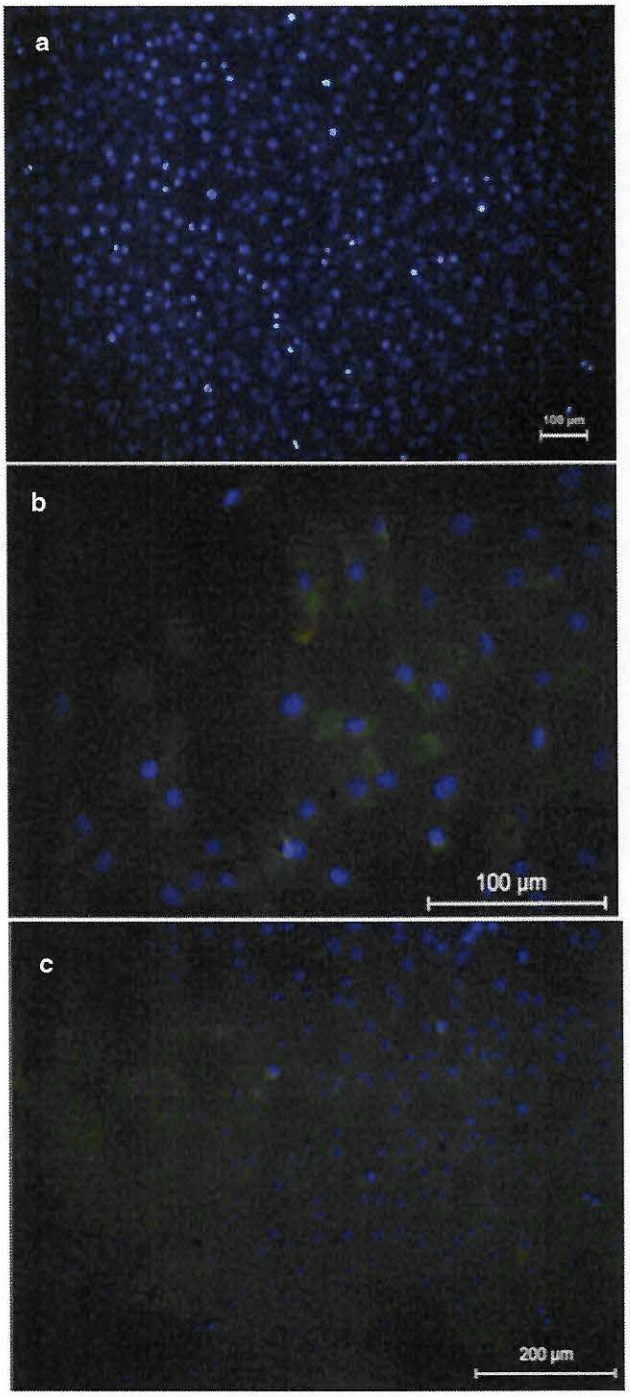

Fig. 5 – SEM of morphology of the cells adhered to the mullite surface.

5% CO_2 atmosphere for 4 h. 2 mL of DMEM culture medium was added to each well and the samples remained again under the initial conditions for 72 h. The culture medium was withdrawn from the wells; for the MTT test, each cylinder was gently washed with PBS and 2 mL of MTT (0.5 mg/mL in PBS) were added to each well. The microplates were protected from light and incubated at 37 ± 2 °C for 4 h in 5% CO_2 atmosphere. The cylinders were removed from the wells and washed with PBS. The formazan crystals formed on the surface of the cylinders were solubilized in DMSO (100 µL per well) and the absorbance was read at 570 nm in an ELISA microplate reader (Polaris-Celer spectrophotometer). The viability assays were performed in triplicate. The DMEM culture medium was used as the negative control and the DMSO solution (25 vol% in DMEM) was the positive control. The cell viability was reported in percentage relative to the negative control, calculated using the optical density of the negative control and the optical density of each sample.

Human cell adhesion – The ceramic cylinders were immersed into the wells of 24-well plates. The cells (1.5×10^4 cells/mL, 1 mL) were seeded on the surface of each cylinder, and kept in the oven (at 37 ± 2 °C and 5% CO_2 atmosphere) for 4 h. This first step was performed to allow the cells to adhere at the surface of the samples. Then, 2 mL of DMEM culture medium were added to each well. The samples were incubated again in the oven (at 37 ± 2 °C and 5% CO_2 atmosphere) for 72 h, to allow the cells grow and proliferate at the surface of the samples. After 72 h-incubation, the cells were fixed with glutaraldehyde solution (2.5 vol%) for 40 min at 8 °C, washed with distilled water and dehydrated using increasing ethanol concentration (25, 50, 75 and 100 vol%). Their adhesion to the mullite surface was assessed by SEM and fluorescence microscopy. For SEM, the samples were coated with evaporated carbon in a sputter (Q150R Quorum Technologies, UK) and analyzed under a FEI Inspect F50, Netherlands microscope. Optical fluorescence microscopy was carried out under a LeicaDM 750 fluorescence digital microscope. For staining the cells, mullite was immersed into 1 µg/mL DAPI solution (10 mL) for 10 min, washed with PBS and then immersed in 5 µg/mL FITC solution (10 mL), washed with PBS solution and analyzed by fluorescence microscopy using a green and red filter for DAPI and blue and red filter for FTIC.

The ceramic and all materials used in the experiment were sterilized for 20 min in an autoclave at 121 °C.

3. Results

3.1. *Characterization of the raw materials and mullite*

Table 1 shows the results of the characterization of the raw materials regarding typical density, total pore volume, specific surface area, pore diameter and purity. The morphology of microsilica particles assessed by SEM and TEM is shown in Fig. 2, and the images indicate spherical morphology for the particles and an average diameter ranging from 50 to 500 nm.

The XRD diffraction pattern of mullite is shown in Fig. 3. The main peak that corresponds to mullite ($3Al_2O_3{\cdot}2SiO_2$, file JCPDS no. 15-0776) appears at 26°, according to the literature [29]. The reaction of silica with alumina at 1500 °C led to the formation of mullite (M peaks), as shown by XRD analysis, Fig. 3. The corundum (C peaks) and cristobalite (S peak) peaks indicate the presence of unreacted starting materials, silica and alumina, respectively. Rietveld refining showed crystalline phases of alumina (corundum: 26.32 wt%; 21.59 vol%), crystalline silica (cristobalite: 0.046 wt%; 0.066 vol%) and mullite (73.62 wt%; 78.33 vol%).

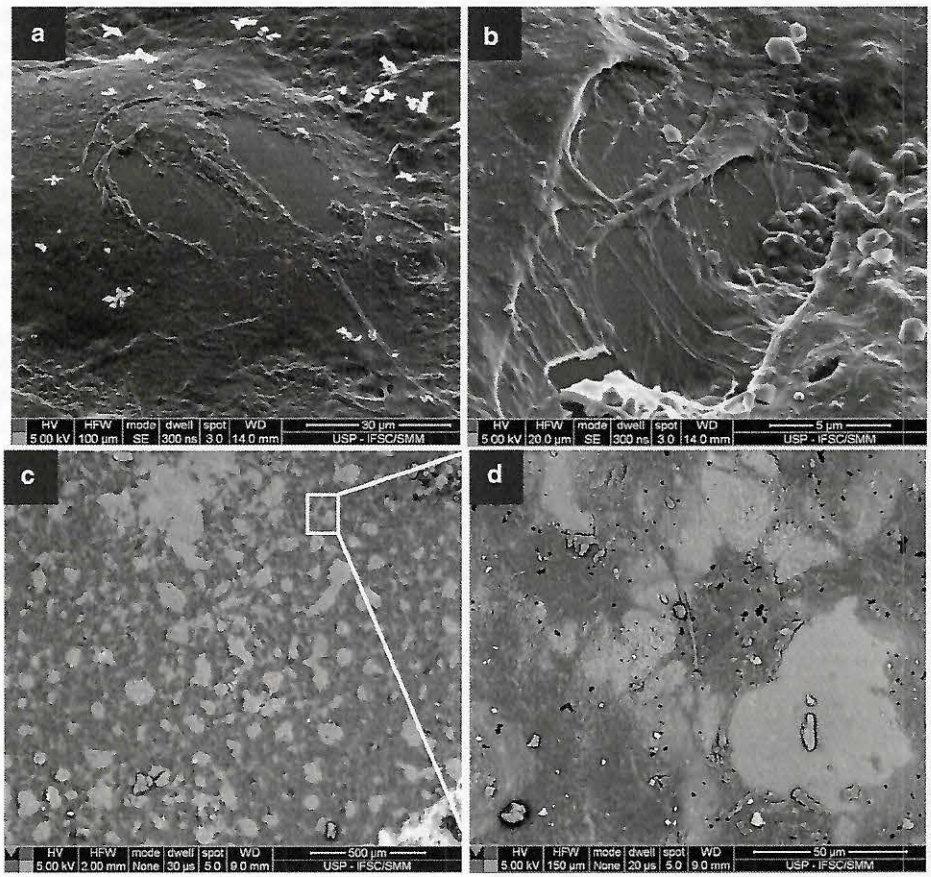

Fig. 6 – Images of the fluorescence of the cells adhered to the surface of the mullite sample: (a) nucleus stained with DAPI (blue), (b) spread morphology of the cells and (c) confluence layer of cells on the surface of the mullite and (d) the magnification of a cell from the confluence layer.

The SEM images (Fig. 4) show the morphology of the material treated at 1500 °C, which appears as a homogeneous sintered material (Fig. 4a and b), as expected for the solid state reaction with concomitant diffusion of the reagents.

3.2. *Mechanical properties and total geometric porosity*

Table 2 shows the results of the elastic modulus, flexural strength and total geometric porosity of the samples. The samples treated at 1500 °C showed total geometric porosity of 7.8%, which indicates the densification of the material. The densification of the born mullite resulted from the arrangement of the structure at high temperatures at which the particles were sintered and generated the continuous phase. Moreover, the low porosity can be explained by the small dimensions of the particles of the precursor's reagents, which increased the packing and favored the formation of the continuous phase of mullite. The results are in agreement with XRD and SEM and indicate the formation of a dense phase of mullite at 1500 °C.

3.3. *Cell viability (MTT) and cell adhesion on the mullite surface*

The cell viability of the negative control was 100% (±0.06) and for the tested sample it was 87.48% (±0.02), indicating no negative effect of the mullite on the cells' growing capability. According to the international standard ISO 10993-5 [32], a cell viability higher than 70% in comparison to the negative control indicates good biocompatibility.

The images assessed by fluorescence microscopy (Fig. 5) show a large number of cells on the mullite surface and their spread morphology. Fig. 5a displays the blue nuclei of the cells marked with DAPI, thus indicating the high number of cells on the mullite surface. Fig. 5b shows the nuclei marked with DAPI (blue) and the cytoplasm of the cells marked with FITC (green). The spread morphology of the cells (Fig. 5b indicated by arrows) and their confluent monolayer (Fig. 5c), shown by the green cytoskeleton, indicating the cells adhered and proliferated on the mullite surface. The spread morphology of the cells is also an indicative of their viability, in good agreement with the MTT results.

The spread morphology of an isolated cell assessed by SEM microscopy is shown in Fig. 6a. The isolated cell is fully adhered to the mullite surface. This is confirmed by SEM, as shown in Fig. 6b, whose magnified image indicates the interaction of the cell's (pseudopods) extension anchored to the mullite surface, confirmed by SEM back scattering mode (Fig. 6c and d), where the cells appeared dark and the mullite appears clear. Fig. 6c shows the overall aspect of the sample almost covered by cells (dark area) and Fig. 6d displays the magnification of the cell from Fig. 6c with spread morphology.

4. Discussion

The reaction for mullite formation can be affected by parameters, such as particle size of precursors, presence of impurities, heating rate, temperature of thermal processing and nature of the silica source. The latter is one of the main variables that affect the yield, kinetics of the reaction and morphology of the products [33]. The composition of the raw material (Table 1) revealed substances other than silica, such as calcium and potassium, known as liquid phase formers. They improved the formation of viscous mass and increase the wettability of the material, i.e., silica wets alumina, increasing the reactivity of the system for benefiting the formation of mullite [29,34,35]. Regarding morphology, in general, high reactivity is expected for small diameter particles (Fig. 2). The diameter of silica and its amorphous structure are important properties that can favor packing. The small dimension of microsilica tends to accelerate the mullite formation process and to be carried out at low temperatures representing a potential former of mullite phase. The process generates high-density and low-porosity mullite phases. Fig. 4 shows SEM images of mullite fracture; the morphology indicates the formation of a viscous material resulting from the wetting of silica by alumina, favored by the liquid phase sintering, as expected. Such results are in agreement with the XRD data (Fig. 3), which indicate the formation of the mullite phase [34].

The densification of the samples in the sintering process improved their mechanical properties, which is important for biomedical applications, see Table 2. For instance, it is mainly related to loading distribution for bone replacement. In general, the elastic modulus of mullite (Table 2) is higher than the elastic modulus of cortical bones (approximately 20 GPa) [36], suggesting its use as potential material for bone replacement. Most ceramic implants are usually developed for hip joint arthroplasty, however there is also a demand for implants of smaller bones that does not demand high mechanical loading, such as radial head in elbow, which could represent an alternative field for the mullite application. The results of cell viability in the presence of mullite are indicative of the biocompatibility of the material, supported by the adhesion studies on their surface, and these results suggest its potential for use in bone replacement.

5. Conclusions

Mullite was formulated and prepared *via* sintering reaction by heat treatment at 1500 °C, showing low porosity and high density resulting in a material with suitable mechanical properties. Its nature enabled GM07492 cells to survive and proliferate when sown on the surface of the material, as demonstrated by the *in vitro* cell viability and adhesion tests. The results of the first level of evidence studies (*in vitro* cytotoxicity tests) showed the absence of cytotoxicity and proliferation of cells at the surface of mullite, which represent an important step for future complementary pre-clinical and clinical studies.

Conflicts of interest

The authors declare no conflicts of interest.

Acknowledgements

The authors acknowledge CNPq for the PhD grant awarded to L.F. (142372/2014-5), FAPESP (2010/19274-5), CNPq 870346/1997-0, Almatis (Brazil and Germany), Elkem (Norway). They are also indebted Rafael Paiotti M. Guimarães (Evaluation and Interpretation of Rietveld method) and Wagner R. Correr MSc. (Microscopy Laboratory CTMH SMM-EESC/IFSC) for SEM images.

REFERENCES

[1] Charnley J. Arthroplasty of the hip: a new operation. Lancet 1961;1:1129–32, http://dx.doi.org/10.1016/S0140-6736(61)92063-3.
[2] Smerdelj M, Orlić D, Bergovec M. Emergencies in total hip replacement. Lijec Vjesn 1989;127:189–93.
[3] Miyazaki T, Nakamura T, Matsumura H, Ban S, Kobayashi T. Current status of zirconia restoration. J Prosthodont Res 2013;57:236–61, http://dx.doi.org/10.1016/j.jpor.2013.09.001.
[4] Chevalier J, Gremillard L. Ceramics for medical applications: a picture for the next 20 years. J Eur Ceram Soc 2009;29:1245–55, http://dx.doi.org/10.1016/j.jeurceramsoc.2008.08.025.
[5] Pezzotti G. Bioceramics for hip joints: the physical chemistry viewpoint. Materials (Basel) 2014;7:4367–410, http://dx.doi.org/10.3390/ma7064367.
[6] Patel N, Gohil P. A review on biomaterials: scope, applications & human anatomy significance. Int J Emerg Technol Adv Eng 2012;2:91–101.
[7] Maccauro G, Piconi C, Burger W, Pilloni L, De Santis E, Muratori E, et al. Fracture of a Y-TZP ceramic femoral head. J Bone Jt Surg – Br Vol 2004;86B:1192–6, http://dx.doi.org/10.1302/0301-620x.86b8.15012.
[8] Chevalier J, Gremillard L, Virkar AV, Clarke DR. The tetragonal–monoclinic transformation in zirconia: lessons learned and future trends. J Am Ceram Soc 2009;92:1901–20, http://dx.doi.org/10.1111/j.1551-2916.2009.03278.x.
[9] Chevalier J, Gremillard L, Deville S. Low-temperature degradation of zirconia and implications for biomedical implants. Annu Rev Mater Res 2007;37:1–32, http://dx.doi.org/10.1146/annurev.matsci.37.052506.084250.
[10] Chevalier J. What future for zirconia as a biomaterial? Biomaterials 2006;27:535–43, http://dx.doi.org/10.1016/j.biomaterials.2005.07.034.
[11] Rodriguez-Gonzalez FÁ. Introduction to biomaterials in orthopaedic surgery. Biomater Orthop Surg 2009:1–10, http://dx.doi.org/10.1142/9789812700858.
[12] Affatato S, Ruggiero A, Merola M. Advanced biomaterials in hip joint arthroplasty. A review on polymer and ceramics

composites as alternative bearings. Compos Part B: Eng 2015;83:276–83, http://dx.doi.org/10.1016/j.compositesb.2015.07.019.
[13] McEntire BJ, Bal BS, Rahaman MN, Chevalier J, Pezzotti G. Ceramics and ceramic coatings in orthopaedics. J Eur Ceram Soc 2015;35:4327–69, http://dx.doi.org/10.1016/j.jeurceramsoc.2015.07.034.
[14] Schneider H, Schreuer J, Hildmann B. Structure and properties of mullite – a review. J Eur Ceram Soc 2008;28:329–44, http://dx.doi.org/10.1016/j.jeurceramsoc.2007.03.017.
[15] Pezzotti G, Yamamoto K. Artificial hip joints: the biomaterials challenge. J Mech Behav Biomed Mater 2014;31:3–20, http://dx.doi.org/10.1016/j.jmbbm.2013.06.001.
[16] Anggono J. Mullite ceramics: its properties structure, and synthesis. J Tek Mesin 2005;7:1–10, http://dx.doi.org/10.9744/jtm.7.1.
[17] Sousa LL, Souza ADV, Fernandes L, Arantes VL, Salomão R. Development of densification-resistant castable porous structures from in situ mullite. Ceram Int 2015;41:9443–54, http://dx.doi.org/10.1016/j.ceramint.2015.03.328.
[18] Fernandes L, Salomão R. Preparation and characterization of mullite-alumina structures formed "in situ" from calcined alumina and different grades of synthetic amorphous silica. Mater Res 2018;21, http://dx.doi.org/10.1590/1980-5373-MR-2017-0783.
[19] Yang F, Li C, Lin Y, Wang C-A. Effects of sintering temperature on properties of porous mullite/corundum ceramics. Mater Lett 2012;73, http://dx.doi.org/10.1016/j.matlet.2011.12.087.
[20] Deng Z-Y, Fukasawa T, Ando M, Zhang G-J, Ohji T. Microstructure and mechanical properties of porous alumina ceramics fabricated by the decomposition of aluminum hydroxide. J Am Ceram Soc 2001;84:2638–44, http://dx.doi.org/10.1111/j.1151-2916.2001.tb01065.x.
[21] Ducheyne P, Healy KE, Grainger DW, Hutmacher DW, Kirkpatrick CJ. Comprehensive biomaterials, vol. 1; 2011, http://dx.doi.org/10.1016/C2009-1-28384-5.
[22] Nath S, Dubey AK, Basu B. Mechanical properties of novel calcium phosphate–mullite biocomposites. J Biomater Appl 2012;27:67–78, http://dx.doi.org/10.1177/0885328210393292.
[23] Goodridge RD, Wood DJ, Ohtsuki C, Dalgarno KW. Biological evaluation of an apatite–mullite glass-ceramic produced via selective laser sintering. Acta Biomater 2007;3:221–31, http://dx.doi.org/10.1016/j.actbio.2006.10.005.
[24] Nath S, Basu B, Mohanty M, Mohanan PV. In vivo response of novel calcium phosphate–mullite composites: results up to 12 weeks of implantation. J Biomed Mater Res Part B: Appl Biomater 2009;90B:547–57, http://dx.doi.org/10.1002/jbm.b.31316.
[25] Kalmodia S, Sharma V, Pandey AK, Dhawan A, Basu B. Cytotoxicity and genotoxicity property of hydroxyapatite–mullite eluates. J Biomed Nanotechnol 2011;7:74–5, http://dx.doi.org/10.1166/jbn.2011.1208.
[26] Fernandes L, De Arruda CC, Souza ADV, Salomão R. Characterization of synthetic amorphous silica (SAS) used in the ceramics industry. InterCeram – Int Ceram Rev 2014;63:220–4.
[27] ISO 6872:2015. Dentistry – ceramic materials. Int Organ Standardization 2015; 2015.
[28] Mccusker LB, Dreele RB Von, Cox DE, Loue ÈRDD, Scardi P. Rietveld refinement guidelines. Int Union Crystallogr, J Appl Crystallogr J Appl Cryst 1999;32:36–50, http://dx.doi.org/10.1107/S0021889898009856.
[29] Fernandes L, Salomão R. Preparation and characterization of mullite-alumina structures formed "in situ" from calcined alumina and different grades of synthetic amorphous silica. Mater Res 2018, http://dx.doi.org/10.1590/1980-5373-mr-2017-0783.
[30] Ramay HR, Zhang M. Preparation of porous hydroxyapatite scaffolds by combination of the gel-casting and polymer sponge methods. Biomaterials 2003;24:3293–302, http://dx.doi.org/10.1016/S0142-9612(03)00171-6.
[31] Priya A, Nath S, Biswas K, Basu B. In vitro dissolution of calcium phosphate–mullite composite in simulated body fluid. J Mater Sci Mater Med 2010;21:1817–28, http://dx.doi.org/10.1007/s10856-010-4053-1.
[32] International Organization for Standardization. Biological evaluation of medical devices. Part 5: Tests for in vitro cytotoxicity; 2009.
[33] Bartsch M, Saruhan B, Schmucker M, Schneider H. Novel low-temperature processing route of dense mullite ceramics by reaction sintering of amorphous SiO_2-coated γ-Al_2O_3 particle nanocomposites. J Am Ceram Soc 1999;82:1388–92, http://dx.doi.org/10.1111/j.1151-2916.1999.tb01928.x.
[34] Saruhan B, Albers W, Schneider H, Kaysser WA. Reaction and sintering mechanisms of mullite in the systems cristobalite/[alpha]-Al_2O_3 and amorphous SiO_2/alpha-Al_2O_3. J Eur Ceram Soc 1996;16:1075–81.
[35] Fernandes L, De Arruda CC, Souza ADV, Salomão R. Synthetic amorphous silica (SAS) used in the ceramics industry. Keram Z 2014;66.
[36] de Sousa LL, Salomão R, Arantes VL. Development and characterization of porous moldable refractory structures of the alumina–mullite–quartz system. Ceram Int 2017;43:1362–70, http://dx.doi.org/10.1016/j.ceramint.2016.10.093.